Theory of high-temperature superconductivity in underdoped cuprates; the unusual electronic structure and the origin of the pseudogap

1998 J. Phys.: Condens. Matter 10 11345

(http://iopscience.iop.org/0953-8984/10/49/023)

J. Phys.: Condens. Matter **10** (1998) 11345–11364. Printed in the UK PII: S0953-8984(98)96500-6

Theory of high-temperature superconductivity in underdoped cuprates; the unusual electronic structure and the origin of the pseudogap

Hiroshi Kamimura, Kazushi Nomura and Akihiro Sano†

Institute of Physics, Graduate School of Science, Science University of Tokyo, 1-3 Kagurazaka, Shinjuku-ku, Tokyo 162-8601, Japan

Received 3 June 1998

Abstract. By reviewing the first-principles studies of the many-electron electronic structures of underdoped $La_{2-x}Sr_xCuO_4$ and $YBa_2Cu_3O_7$ performed by Kamimura and co-workers, unusual electronic states are clarified. That is, the dopant holes move coherently by taking the Zhang–Rice spin singlet and Hund's coupling spin triplet alternately in the spin-correlated region of antiferromagnetic ordering due to the Cu localized spins, without destroying the antiferromagnetic order. This creates a metallic state which leads to superconductivity. The coexistence of (i) the antiferromagnetic spin ordering and (ii) the ordering in the appearance of the Zhang–Rice singlet and the Hund's coupling triplet results in the small Fermi surface for a carrier system and also leads to the decrease in the electronic entropy below a certain temperature at which the Fermi surface changes from a larger one to smaller ones. This is the microscopic origin of the pseudogap, the concept of which was originally proposed by Loram and co-workers in terms of the Fermi liquid picture.

1. Introduction

The discovery of high-temperature superconductivity in cuprates by Bednorz and Müller [1] has led to an intensive search for the mechanism of the superconductivity. Anderson [2] first pointed out the important role of electron correlation in the mechanism of the superconductivity. Since then, a number of theoretical models have been proposed [3, 4]. Most of them are based on a Cu $d_{x^2-y^2}$–O p_σ hybridized band in a CuO_2 layer, while Kamimura *et al* [5, 6] insisted that the Hund coupling spin-triplet state based on a Cu d_{z^2}–in-plane O p_σ and apical O p_z hybridized band plays an important role in $La_{2-x}Sr_xCuO_4$ (abbreviated as LaSCO) when the average distance between apical oxygen and Cu in the CuO_6 octahedra decreases with increasing Sr concentration so as to lower the total electrostatic energy [7]. The theoretical prediction of the contraction of the Cu–apical O distance made by Shima *et al* [7] has been experimentally verified by recent neutron diffraction experiments by Egami *et al* [8] for LaSCO and other copper oxides, and by Cava *et al* [9] and Shmahl *et al* [10] for YBCO.

Before the neutron experiments were carried out, Boyce *et al* [11] had already pointed out for the first time the contraction of the Cu–apical O distance upon Sr doping, on the basis of the EXAFS experiments. Taking into account these facts, Kamimura and Eto [12]

† Present address: Hitachi Limited, Hitachi Reseach Laboratory, 1-1 Omika-cho 7-chome, Hitachi-shi, Ibaraki-ken, 319-1221, Japan.

0953-8984/98/4911345+20$19.50

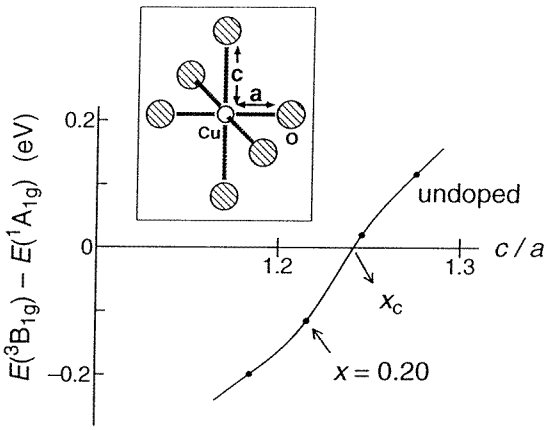

Figure 1. The energy difference between the $^1A_{1g}$ and $^3B_{1g}$ states in $La_{2-x}Sr_xCuO_4$ calculated by the MCSCF variational methods as a function of the apical O–Cu distance, where the Cu–apical O distance of a CuO_6 octahedron, c (see the inset of the figure), changes according to the hole concentration x (after Kamimura and Eto (reference [12])). Thus the hole concentration corresponding to a value of c is also indicated. When x reaches x_c, the $^3B_{1g}$ state becomes the lowest, where x_c lies at around 0.1 in the underdoped region.

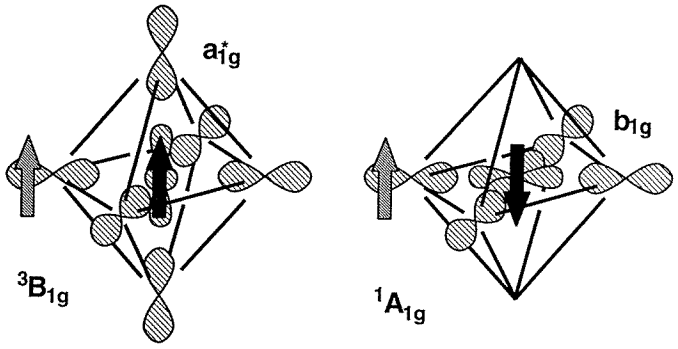

Figure 2. Schematic views of the $^1A_{1g}$ and $^3B_{1g}$ multiplet states in a CuO_6 octahedron, together with views of the spatial extents of the a^*_{1g} and b_{1g} orbitals. Hatched and solid arrows represent the spin of a carrier and a localized Cu spin, respectively.

performed a multi-configuration self-consistent-field (MCSCF) variational calculation with configuration interactions (CI) to determine the ground state of a CuO_6 octahedron embedded in LaSCO for various Sr concentrations, and showed that the ground state changes from the spin-singlet state, $^1A_{1g}$, to the spin-triplet state, $^3B_{1g}$, in the underdoped region, when the Sr concentration increases, where A_{1g} and B_{1g} represent irreducible representations of a tetragonal symmetry group, D_{4h}. (Hereafter we call the many-electron electronic states such as $^1A_{1g}$, $^3B_{1g}$, etc, 'multiplets'.) The results calculated by Kamimura and Eto [12] are shown in figure 1, where the energy difference between the $^1A_{1g}$ and $^3B_{1g}$ multiplets is plotted as a function of the apical O–Cu distance c, with the Cu–O distance a in a CuO_2 plane being kept constant. As shown in figure 2, the dopant holes in the $^1A_{1g}$ multiplet occupy a bonding b_{1g} orbital consisting of the in-plane oxygen p_σ orbitals hybridized with a Cu $d_{x^2-y^2}$ orbital while in the $^3B_{1g}$ multiplet they occupy an antibonding a^*_{1g} orbital consisting of a Cu

d_{z^2} orbital hybridized with the in-plane oxygen p_σ and the apical oxygen p_z orbitals, in the presence of a localized spin of $S = 1/2$ around Cu sites which is due to the effect of strong electron correlation. These $S = 1/2$ localized spins give rise to antiferromagnetic two-dimensional spin ordering due to the superexchange interactions via intervening oxygen ions over a region of the spin-correlation length, when the CuO_6 octahedra compose a periodic arrangement in CuO_2 layers.

As seen in figure 1, the $^3B_{1g}$ state in $La_{2-x}Sr_xCuO_4$ is lowered by only 0.1 eV even for $x = 0.2$ as compared with the $^1A_{1g}$ state, so the transfer interactions between neighbouring CuO_6 octahedra, which are of the order of 0.3 eV, make these two states mixed in the underdoped superconducting state. In view of this, Kamimura and Ushio [13] constructed many-electron energy bands for LaSCO in such a way as to allow the coexistence of the $^1A_{1g}$ and $^3B_{1g}$ states.

In order to investigate the existence of the $^3B_{1g}$ state, Chen *et al* [14] performed polarization-dependent x-ray absorption measurements for O K and Cu L edges in LaSCO. For the Cu L edge, they observed the doping-induced satellite peak (L_3') for both polarizations of the electric vector of the x-rays $\boldsymbol{E}$, parallel and perpendicular to the *c*-axis, in a shoulder area of the doping-independent Cu L_3 line with the intensity ratio of about 1 to 9, where the L_3 line corresponds to transitions from the Cu 2p core level to the upper Hubbard Cu $d_{x^2-y^2}$ band, indicating the existence of localized spins. Since the former ($\boldsymbol{E} \parallel \boldsymbol{c}$) and the latter ($\boldsymbol{E} \perp \boldsymbol{c}$) polarizations detect high-spin ($^3B_{1g}$) and low-spin ($^1A_{1g}$) multiplets, respectively, the appearance of the doping-induced satellite peak for both polarizations at the same energy suggested that the state of the dopant holes must be a single coherent state consisting of high- and low-spin states. For the compounds $Tl_2Ba_2CaCu_2O_8$ and $Tl_2Ba_2Ca_2Cu_3O_3$ as well as LaSCO, Pellegrin *et al* [15] have also found polarization dependence, similar to that found by Chen *et al* [14].

In 1989 Bianconi *et al* [16] also reported that the peak energy separation between transitions for polarizations parallel and perpendicular to the *c*-axis in LaSCO decreases towards zero when the Sr concentration increases from a non-superconducting regime to a superconducting regime, consistently with the above experimental results.

The existence of localized spins on Cu indicated by the observation of the Cu L_3 line is also supported by neutron scattering experiments. For example, Birgeneau *et al* [17] showed the coexistence of the spin correlation of localized spins and superconductivity in LaSCO; that is, the spins of Cu $d_{x^2-y^2}$ holes form a two-dimensional local antiferromagnetic (AF) order even in the superconducting state. Then Kamimura and Suwa [18] pointed out that the dopant holes may move coherently over a long distance without destroying the local AF order, when the dopant holes take high- and low-spin multiplets alternately in a region of antiferromagnetically coupled localized spins.

They proposed a coupled spin-fermion-type effective Hamiltonian describing the above unusual electronic structure. Then Kamimura and Ushio [13, 19] constructed the many-electron energy bands, Fermi surfaces, and the density of states by solving approximately the effective Hamiltonian proposed by Kamimura and Suwa. Using these energy bands, Fermi surfaces, and the density of states including the many-body effect, Kamimura *et al* [20] investigated the mechanism of superconductivity in hole-doped copper oxides, and recently they showed quantitatively that the electronic structures calculated by Kamimura and Ushio create a d-wave pairing even in the phonon mechanism. Then Matsuno *et al* [21] calculated the hole concentration dependence of the superconducting transition temperature in LaSCO and found good agreement with experimental results given by Takagi *et al* [22].

In this article we first extend the calculation carried out by Kamimura and Eto [12] to a CuO_5 pyramid embedded in superconducting $YBa_2Cu_3O_7$ (abbreviated as $YBCO_7$) with

$T_c = 90$ K. For this purpose we first describe a cluster model for a CuO_5 cluster in $YBCO_{7-\delta}$ in section 2. In section 3 we briefly review the MCSCF-CI method. In section 4 the calculated results are presented. In particular, an important role of the charge-density wave in a Cu–O chain in determining the electronic structure of $YBCO_7$ is clarified. In section 5 the idea put forward by Kamimura and Suwa of constructing the electronic structure in the underdoped superconducting concentration region of the cuprate [18] is reviewed, and then experimental evidence in support of Kamimura and Suwa's idea is presented in section 6. In section 7 the effective Hamiltonian for the Kamimura–Suwa model is presented. In section 8 a method for calculating the many-electron energy bands, wave functions, and Fermi surfaces based on Kamimura and Suwa's idea is introduced, and the results calculated for LaSCO by Ushio and Kamimura [55] are reviewed. Finally, the microscopic origin for the pseudogap is discussed in section 9.

2. The cluster model

2.1. The model for CuO_5 in $YBa_2Cu_3O_{7-\delta}$

As a model for cluster calculations, we adopt a single CuO_5 pyramid embedded in the compound $YBa_2Cu_3O_{7-\delta}$ (abbreviated as $YBCO_{7-\delta}$ hereafter). We label the oxygens in the CuO_2 plane as O(1), and the apical oxygens as O(2). We use the lattice constants reported by Cava *et al* for $YBCO_{7-\delta}$ [23]. The number of electrons is determined such that the formal charge of copper is $+2e$ and that of oxygen is $-2e$ for the undoped case. We also consider the hole-doped system for $YBCO_{7-\delta}$ by subtracting one electron.

To include the effect of the Madelung potential from the ions outside the cluster, the point charges are placed at exterior-ion sites ($+2e$ for Cu and Ba, $-2e$ for O, and $+3e$ for Y). The number of point charges is 300 to 1400 for CuO_5, depending on the distribution of the charges of the Cu ions in the Cu–O chains. These point charges determine the Madelung potential at Cu, O(1), and O(2) sites within the cluster in such a way that the relative value of the Madelung potential at each site is reproduced so as to coincide with that for the purely ionic crystal, within less than a few eV.

For the case of a CuO_6 cluster in LaSCO, we have varied the Cu–O(2) distance c according to the experimental results given by Boyce *et al* [11] and to the theoretical results given by Shima *et al* [7]. The distance c is taken as 2.41 Å, 2.35 Å, 2.30 Å, and 2.24 Å, depending on the Sr concentration, where 2.41 Å and 2.30 Å correspond to the values of c for the compounds with $x = 0$ (undoped) and $x = 0.2$, respectively, in the $La_{2-x}Sr_xCuO_4$ series. In the case of a CuO_5 cluster, on the other hand, the Cu(2)–O(2) distance is taken as 2.47 Å for $YBCO_6$ and 2.29 Å for $YBCO_7$, following the experimental results obtained by neutron [9] and x-ray [10] diffraction measurements, where Cu(2) represents the Cu ions in the CuO_2 planes while Cu(1) represents the Cu(1) ions in the Cu–O chains.

2.2. The basis set

We express the one-electron orbitals as linear combinations of atomic orbitals; Cu 1s, 2s, 3s, 4s, 2p, 3p, 3d and O 1s, 2s, 2p orbitals are taken into account as the atomic orbitals. Each atomic orbital is represented as a linear combination of several Gaussian functions. For Cu 3d, 4s and O 2s, 2p atomic orbitals we prepare two basis functions called 'double-zeta' functions for each orbital. These are (12s6p4d)/[5s2p2d] for Cu [24] and (10s5p)/[3s2p] for O [25].

As to the oxygen ions, the diffuse components are usually used by researchers in

quantum chemistry. The diffuse components, however, cause problems with the point charge approximation outside of the cluster when a cluster is embedded in a crystal, because the diffuse components reach the nearest-neighbour sites with considerable amplitudes. Hence we do not use the diffuse components, although other groups have used them in their cluster calculations for the copper oxide superconductors [26–28]. Instead of using the diffuse components for O^{2-}, we use extended O 2p basis functions which were originally prepared for neutral atoms, by introducing a scaling factor of 0.93. We multiply all of the Gaussian exponents in the double-zeta basis for the oxygen 2p orbitals by the same scaling factor. The value of the scaling factor is determined such that the energy of an isolated O^{2-} ion should be minimized in the Hartree–Fock approximation.

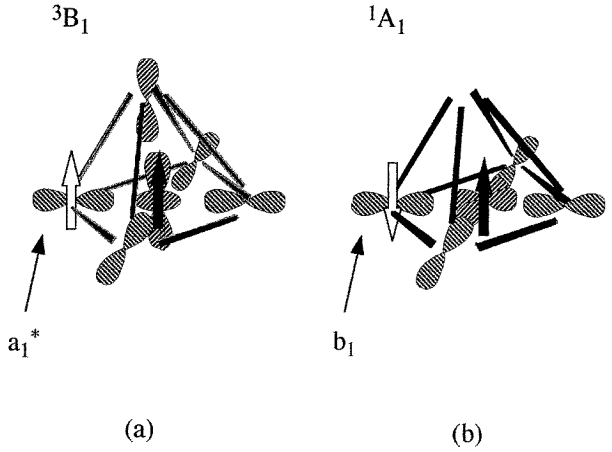

Figure 3. A schematic view of a $^3B_1$ multiplet (a) and a $^1A_1$ multiplet (b) in a CuO_5 pyramid. A solid arrow represents a localized spin while an open arrow represents the spin of a hole carrier which occupies an antibonding a_1^* orbital shown in the figure. The spatial extents of the antibonding a_1^* orbital and of the bonding b_1 orbital are also shown in this figure.

2.3. The $^1A_1$ and $^3B_1$ multiplets

Like for LaSCO, when holes are doped in $YBCO_{7-\delta}$ there are two possibilities as regards orbitals to accommodate a dopant hole in CuO_5. One case is that in which a dopant hole occupies an antibonding a_1^* orbital consisting of a Cu d_{z^2} orbital and five surrounding oxygen p_σ orbitals, and its spin becomes parallel to a localized spin of $S = 1/2$ around a Cu site, by Hund's coupling. This multiplet is denoted by $^3B_1$, as shown in figure 3(a). We call this spin-triplet state 'the Hund's coupling triplet'. The other case is that in which a dopant hole occupies a bonding b_1 orbital consisting of in-plane oxygen p_σ orbitals with a small Cu $d_{x^2-y^2}$, component and its spin becomes anti-parallel to the localized spin as shown in figure 3(b). This multiplet is denoted by $^1A_1$. Since the t–J model given by Zhang and Rice [29] is based on this $^1A_1$ multiplet, we call this spin-singlet multiplet 'the Zhang–Rice singlet'. Later we calculate the lowest-state energies of the $^3B_1$ and the $^1A_1$ multiplets by the variational method, and determine which of these two multiplets is the lowest in superconducting $YBCO_7$.

3. The multi-configuration self-consistent-field method with configuration interaction (MCSCF-CI method)

We calculate the electronic structure in a CuO_5 pyramid or CuO_6 octahedron cluster by the MCSCF-CI method. In this section we give a brief review of how to use this method for the calculations of the lowest-state energies of the $^1A_1$ (or $^1A_{1g}$ in the case of a CuO_6 octahedron) and $^3B_1$ (or $^3B_{1g}$) multiplets. First, we determine the one-electron orbitals by the MCSCF variational method [30–32, 12, 33]. The trial functions are taken for the Zhang–Rice singlet $^1A_1$ (or $^1A_{1g}$) as

$$\Phi_S = C_0|\psi_1\alpha\psi_1\beta\psi_2\alpha\psi_2\beta\cdots\psi_n\alpha\psi_n\beta| + \sum_i\sum_a C_{ii}^{aa}|\cdots\psi_{i-1}\alpha\psi_{i-1}\beta\psi_{i+1}\alpha\psi_{i+1}\beta\cdots\psi_a\alpha\psi_a\beta| \quad (1)$$

and for the Hund's coupling triplet $^3B_{1g}$ (or $^3B_1$) as

$$\Phi_T = C_0|\psi_1\alpha\psi_1\beta\cdots\psi_{n-1}\alpha\psi_{n-1}\beta\psi_p\alpha\psi_q\alpha| + \sum_i\sum_a C_{ii}^{aa}|\cdots\psi_{i-1}\alpha\psi_{i-1}\beta\psi_{i+1}\alpha\psi_{i+1}\beta\cdots\psi_a\alpha\psi_a\beta\psi_p\alpha\psi_q\alpha| \quad (2)$$

where $2n$ is the number of electrons in the clusters, and $|\cdots|$ represents a Slater determinant. The orbitals ψ_p and ψ_q are always singly occupied in equation (2). In equations (1) and (2) all of the two-electron configurations are taken into account in the summation over i and a, so the correlation effect is effectively included in this method. By varying the ψ_i and the coefficients C_0 and C_{ii}^{aa}, we minimize the energy for each multiplet.

Next, we perform the CI calculation, by using the MCSCF one-electron orbitals ψ_i determined above as a basis set, and obtain the lowest energy of a multiplet. Since the main part of the correlation effect has already been included in determining the MCSCF one-electron orbitals, only a small number of Slater determinants are needed to represent the lowest state, and thus we can get a clear view of the many-body states by this MCSCF-CI method, even when the correlation effect is strong. Thus the MCSCF-CI method is the most suitable variational method for a strongly correlated cluster system [32, 12].

In the MCSCF method we consider all of the orbitals consisting of the Cu $3d_{x^2-y^2}$, $3d_{z^2}$, 4s and O $2p_\sigma$ orbitals in the summation over i and a in equations (1) and (2). In the CI calculation, all of the single-electron excitation configurations among these orbitals are taken into account.

4. Calculated results for the CuO_5 pyramid in $YBCO_{7-\delta}$

In this section we present the results calculated for the hole-doped CuO_5 pyramid cluster in superconducting $YBCO_7$. In this case, $2n$ in equations (1) and (2) is 76. For insulating $YBCO_6$, Sano *et al* [34, 35] recently published the calculated result, and thus we omit describing their calculations in this article and simply present the result, together with those for $YBCO_7$. In figure 4(a) the crystal structure of $YBCO_7$ is shown. For comparison, that of insulating $YBCO_6$ is also shown, in figure 4(b). A remarkable difference between the crystal structures of $YBCO_7$ and $YBCO_6$ is that there exists a Cu–O chain in $YBCO_7$. Like for LaSCO, there are two orbitals, an antibonding a_1 orbital, a_1^*, and a bonding b_1 orbital, b_1, as possible orbital states for accommodating dopant holes, where the point group of the CuO_5 pyramid is C_{4v}. Sketches of the spatial extent of the a_1^* and b_1 orbitals are shown in figures 3(a) and 3(b). We have to deal with the $^1A_1$ and $^3B_1$ multiplets independently, following the theoretical method described in section 3. In doing so, we take into account

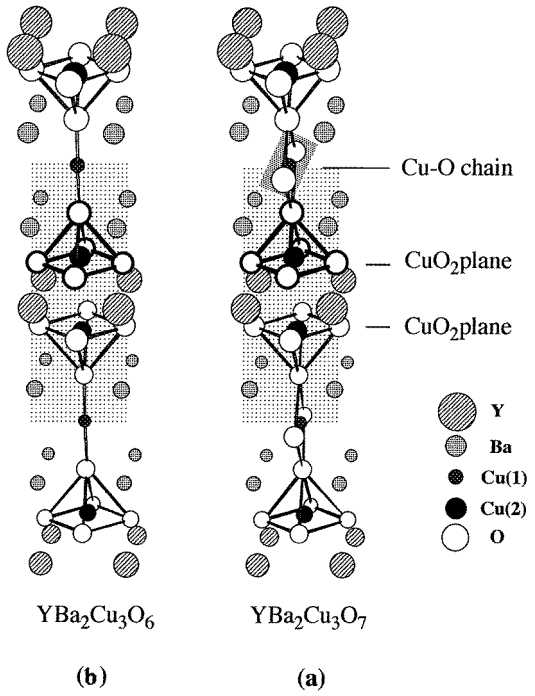

Figure 4. The crystal structures of $YBCO_{7-\delta}$. (a) The orthorhombic structure of superconducting $YBCO_7$. (b) The tetragonal structure of insulating $YBCO_6$.

the effect of the Madelung potential from the ions outside the cluster by placing the point charges $+2$ at Cu(2) in the CuO_2 plane, $+2$ at Ba, $+3$ at Y, and -2 at O. As to the charge of Cu in the Cu–O chain (Cu(1)), q, we have taken $q = +1$ for insulating $YBCO_6$ from the experimental (NMR) result [36]. However, for superconducting $YBCO_7$, the value of q has not been established so far. Thus we calculate the energy difference between the $^1A_1$ and $^3B_1$ multiplets in the case of $YBCO_7$ as a function of q, and then investigate the effect of an inhomogeneous hole distribution in a Cu–O chain on the electronic state, in subsection 4.2.

4.1. The energy difference between the $^1A_1$ and $^3B_1$ multiplets for constant charge of Cu(1) ions in a Cu–O chain

The calculated energy difference between the $^1A_1$ and the $^3B_1$ multiplets in $YBCO_7$ is shown in figure 5, as a function of the charge of Cu(1), q. The value of q and the existence of O^{2-} ions in the Cu–O chain play crucial roles in determining the Madelung energy at the apical O site in a CuO_5 pyramid. Sano *et al* [37] calculated the energy difference between the $^1A_1$ and $^3B_1$ multiplets for insulating $YBCO_6$ to be 1.3 eV, as seen in figure 5 (closed circle), where the distance between Cu(2) and the apical O, c, is fixed at 2.47 Å. In figure 5 the open circles show the energy difference for $YBCO_7$ as a function of q, where c is fixed at 2.29 Å. For $YBCO_7$, it should be recalled that the oxygen ions are introduced to form a Cu–O chain, as seen in figure 4(a). It is clear from figure 5 that, when the value of q decreases, the ground state of the CuO_5 pyramid in $YBCO_7$ changes from $^1A_1$ to $^3B_1$ at around $q \approx 1.45$. This occurs for the following reason: as the value of q decreases, the Madelung potential at the apical oxygen site decreases. As a result, the energy difference

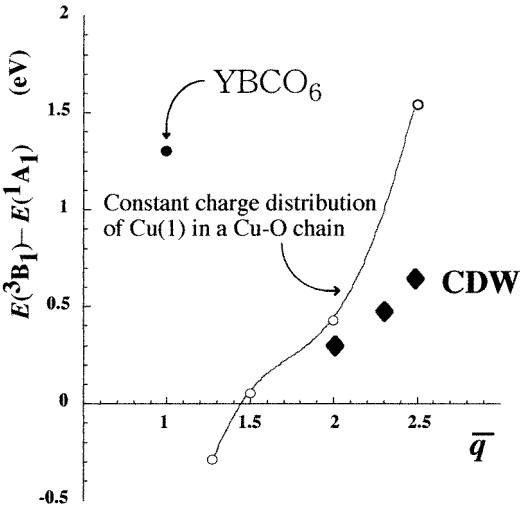

Figure 5. The energy difference between the $^3B_1$ and the $^1A_1$ multiplets, as a function of the charge of a Cu(1) ion in a Cu–O chain, q, in a hole-doped CuO_5 cluster embedded in $YBCO_6$ and $YBCO_7$. The closed circle represents the energy difference between the $^3B_1$ and $^1A_1$ multiplets in $YBCO_6$ [34, 35]. The open circles represent the energy difference between the $^3B_1$ and $^1A_1$ multiplets in superconducting $YBCO_7$ as a function of constant q for all Cu(1) ions, where c is fixed at 2.29 Å. Furthermore, the solid diamonds represent the case of the existence of a CDW in a Cu–O chain, where the results for average values of the charge of the Cu(1) ions, $\bar{q}$, of 2.5, 2.3 and 2.0 are shown [38].

between the energy of the a_1^* orbital which contains the p_z orbital at the apical oxygen site and that of the b_1 orbital becomes smaller, so Hund's coupling becomes more effective.

4.2. The effect of a charge-density wave (CDW) in a Cu–O chain

In a previous subsection we found that, in $YBCO_7$, the calculated lowest-state energy is very sensitive to the charge of Cu(1) in a Cu–O chain, q. In this subsection we investigate how the multiplets of a CuO_5 pyramid are affected by the inhomogeneous hole distribution in a Cu–O chain—that is, the charge-density wave (CDW). Recently the existence of such a CDW in a Cu–O chain in YBCO has been reported by various experimental groups [39–43]. For example, a scanning tunnelling microscopy (STM) experiment [39] and neutron inelastic scattering experiments [40] have shown the existence of a CDW in a Cu–O chain in $YBCO_7$. In this paper we try to clarify theoretically how the CDW in a Cu–O chain affects the electronic structure of the hole-doped CuO_5 pyramid cluster. This is the first theoretical study on the effect of a CDW in a Cu–O chain on the electronic structure of a CuO_5 pyramid.

There is a close connection between the CDW modulation wavelength and the hole concentration in a Cu–O chain. The observed modulation wavelength of a CDW in a Cu–O chain takes a value between 13 and 16 Å. Suppose that the charge of a Cu(1), q, is $+2.5$ and that the states of the holes in a Cu–O chain can be expressed as a one-dimensional energy band. This means that there are 1.5 holes in a Cu–O chain and that three quarters of the energy band for the Cu–O chain is filled by holes. In this case the Fermi wavenumber k_F is given by $\pi/4a$ approximately, where a is a Cu(1)–Cu(1) distance along the chain and is 3.8 Å for $YBCO_7$. Thus the CDW modulation wavelength becomes 15.2 Å, because

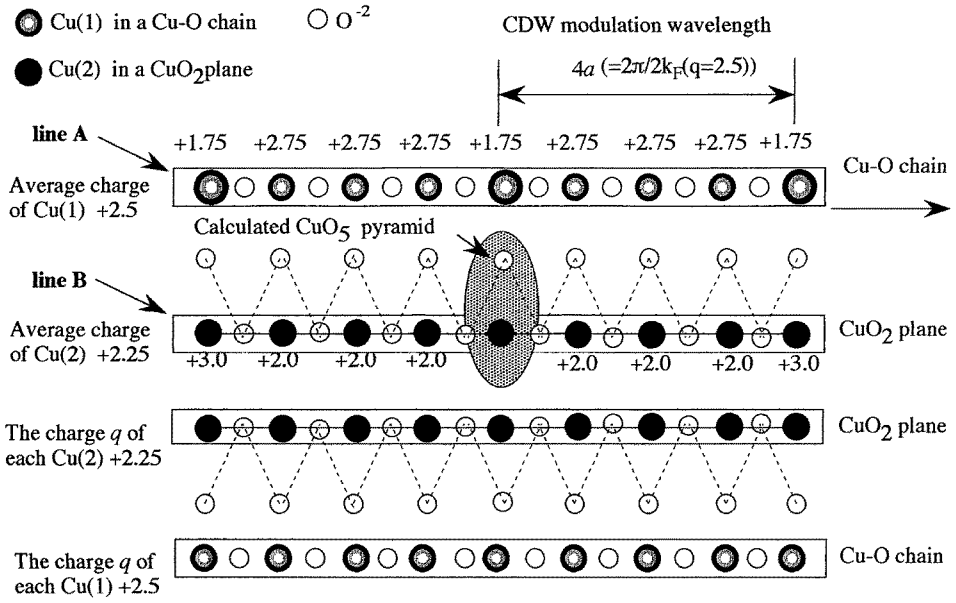

Figure 6. The charge distribution of Cu(1) ions in Cu–O chains and of Cu(2) ions in CuO_2 planes for the case in which the charge of Cu(1) is modulated by the CDW modulation wavelength and the average value of Cu(1)'s charge $\bar{q}$ is equal to 2.5. Line A represents the Cu–O chain which includes the Cu(1) ion immediately above the hatched CuO_5 pyramid under consideration. Line B represents a CuO_2 plane which includes the calculated CuO_5 pyramid.

the modulation wavelength λ_{CDW} is given by $\lambda_{CDW} = 2\pi/2k_F$, and it is nearly equal to $4a$. This value is consistent with the experimental results [39, 40]. In superconducting $YBCO_7$, an oxygen introduced in a Cu–O chain produces two holes in a unit cell consisting of a Cu–O chain and two CuO_2 planes. Considering the charges $+3e$ for Y, $+2e$ for Ba, $+2e$ for Cu(2) and $-2e$ for O in the CuO_2 plane, and $+1e$ for Cu(1) and $-2e$ for O in the Cu–O chain, and further distributing the charge of the dopant holes over a Cu–O chain and two CuO_2 planes in a unit cell, the following equation describes the relationship between the number of holes in the Cu–O chain, η, and that in the CuO_2 plane, ζ, in the unit cell, from the condition of charge neutrality;

$$\eta + 2\zeta = 2. \tag{3}$$

Thus the charge of Cu in a Cu–O chain, q, is related to η by the relation $q = 1 + \eta$. Since the values of η and ζ have not been determined experimentally so far, we calculate the lowest energies of the $^1A_1$ and $^3B_1$ multiplets by varying the value of η. In the case of a uniform charge distribution for the charge of Cu(1) in a Cu–O chain, for example, when we take $q = +2.5$, η becomes 1.5, and thus ζ is 0.25 from equation (3). This means that there is one hole per four CuO_5 pyramids. Since a CuO_5 pyramid cluster is embedded in $YBCO_7$, we must take into account the effect of the Madelung potential from the ions outside the cluster by putting the point charge $+2e$ at Cu(2) in the CuO_2 plane, $+2e$ at Ba, $+3e$ at Y, and $-2e$ at O. As to the charge of Cu(1) in the Cu–O chain, we may place the point charges according to the CDW modulation wavelength, as shown on line A in figure 6. For example, we place $Cu(1)^{1.75+}$ at intervals of every four Cu(1) sites along the line of the Cu–O chain, which corresponds to the Cu(1) immediately above the CuO_5 pyramid cluster under consideration, while we put the charge $+2.75e$ at the remaining Cu(1) sites on line A.

Thus the averaged charge of the Cu(1) atoms on line A is $+2.5e$. In the same way, we put the charge $+3e$ at Cu(2) sites at intervals of four sites with the same modulation as that of the Cu–O chain, and put the charge $+2e$ at the remaining Cu(2) sites on line B in figure 6 which is parallel to line A. Line B includes the CuO_5 pyramid under consideration. Thus the averaged charge of the Cu(2) ions and the averaged hole concentration in a CuO_2 plane on line B become $2.25e$ and 0.25, respectively. As to the charges of all of the Cu(2) ions except those on line B, we take $+2.25e$ as an averaged charge, while as regards the charges of all of the Cu(1) ions except the Cu(1) ions on line A, we take $+2.5e$ as an averaged charge, as shown in figure 6. In this way we consider the CDW-like hole distribution under conditions in which charge neutrality is conserved.

On the basis of the charge distribution shown in figure 6, we have calculated the energies of the $^1A_1$ and $^3B_1$ multiplets by the MCSCF-CI method. The calculated results are shown by solid diamonds in figure 5, where the energy differences between the $^1A_1$ and $^3B_1$ multiplets are shown on the vertical axis, and $\overline{q}$ on the horizontal axis represents the averaged charge of Cu(1) ions in a Cu–O chain. For comparison, we also show the energy difference between the $^1A_1$ and $^3B_1$ multiplets calculated for the case of a constant charge distribution in a Cu–O chain as a function of q [34, 35].

As shown in figure 5, in the case of a constant charge distribution of the Cu(1) ions in the Cu–O chain, the energy difference between $^1A_1$ and $^3B_1$ multiplets is larger than that in the case of a CDW. For example, it is 1.55 eV for $q = +2.5$. As shown by solid diamonds in figure 5, for the case where the CDW hole distribution is taken into account, the calculated energy difference between the $^1A_1$ and $^3B_1$ multiplets is significantly reduced. In the case where $\overline{q} = +2.5$ it becomes 0.65 eV. Thus the electronic structure is strongly affected by the charge distribution in a Cu–O chain caused by the CDW. The decrease of the energy difference between these two multiplets is reasonable, because in this case the Madelung potential at the apical O in a CuO_5 cluster becomes lower for hole carriers. However, since the holes in the Cu–O chains occupy both Cu(1) and O sites, the charge of Cu(1) in a Cu–O chain becomes lower than $+2.5e$. This favours the $^3B_1$ multiplet energetically, because the Madelung potential at the apical O site becomes even lower. Thus we conclude that, when the averaged charge of Cu(1) ions takes a value between 2.0 and 2.3, the energy difference between $^1A_1$ and $^3B_1$ multiplets becomes of the same order of magnitude as the transfer interaction between $^3B_1$ and $^1A_1$ multiplets at neighbouring CuO_5 pyramids, 0.4 eV, because of the existence of the CDW in the Cu–O chain.

5. The Kamimura–Suwa model: electronic structure of underdoped cuprate

Now we construct the many-electron electronic structure of the underdoped cuprates, using the results calculated for a CuO_6 octahedron embedded in LaSCO and for a CuO_5 pyramid in $YBCO_7$. Before presenting the results, we briefly describe the theoretical treatment given by Kamimura and Suwa [18] which we call the Kamimura–Suwa model hereafter. As an example, we choose LaSCO here. According to the Kamimura–Suwa model, there exist areas in each CuO_2 layer in which the localized spins form an antiferromagnetic ordering. These areas are different from an ordinary domain because the boundary of these areas represented by the spin frustration moves by the spin-fluctuation effect. Thus, we call these areas 'spin-correlated regions'. The size of each spin-correlated region is characterized by the spin-correlation length. Then, following the results of Kamimura and Eto [12], a dopant hole with up spin in a spin-correlated region occupies an a_{1g}^* orbital, $\phi_{a_{1g}}$, at CuO_6 octahedra with localized up-spins, because of the energy gain of about 2 eV due to the

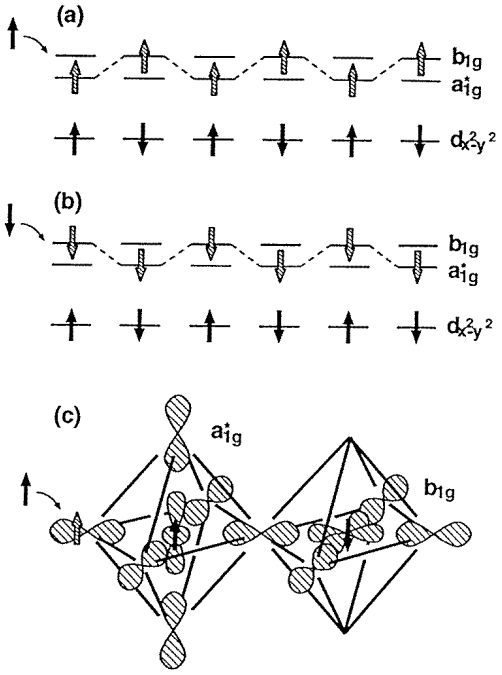

Figure 7. Schematic views of the coherent motion of a dopant hole from high-spin to low-spin states in the presence of antiferromagnetic ordering of the localized spin system. Here (a) and (b) correspond to up-spin and down-spin coherent states of dopant holes, respectively, while (c) represents a coherent motion of an up-spin carrier from a $^3B_{1g}$ to a $^1A_{1g}$ multiplet. It should be noticed that the relative positioning of the a^*_{1g} and b_{1g} levels changes according to the doping concentration. The energy levels in this figure are obtained from the results of Kamimura and Eto (reference [12]).

intra-atomic exchange interaction between the spins of an a^*_{1g} hole and a localized hole in an antibonding b_{1g} orbital (b^*_{1g}) (Hund's coupling) at the same CuO_6 octahedron, as shown in figure 7(c). As a result, the spin-triplet $^3B_{1g}$ state is created. Since Hund's coupling prevents a hole with up spin from occupying an a^*_{1g} orbital in a CuO_6 octahedron with a localized down spin, a hole with up spin cannot hop into a neighbouring a^*_{1g} orbital. Instead, it can enter into a bonding b_{1g} orbital, $\phi_{b_{1g}}$, in a neighbouring CuO_6 octahedron with localized down spin without destroying the antiferromagnetic ordering. In this case there is an energy gain of about 4.0 eV due to the antiferromagnetic exchange interaction between holes in bonding and antibonding b_{1g} orbitals, as shown in figure 7(c). This results in the Zhang–Rice singlet state. In this way the dopant holes can move resonantly from a CuO_6 octahedron to a neighbouring CuO_6 octahedron in a CuO_2 layer by means of a transfer interaction of about 0.3 eV without destroying the local antiferromagnetic (AF) ordering, as shown in figures 7(a) and 7(b). Such coherent motion of the dopant holes is possible when the spin-correlation length is much larger than the distance between neighbouring copper sites and the magnitudes of the transfer interactions between neighbouring CuO_6 clusters are larger than the energy difference between low- and high-spin states. As a result, a metallic state is created, and it simultaneously causes superconductivity, as was shown by Kamimura *et al* [20].

Kamimura and Suwa [18] have expressed the above coherent motion of dopant holes

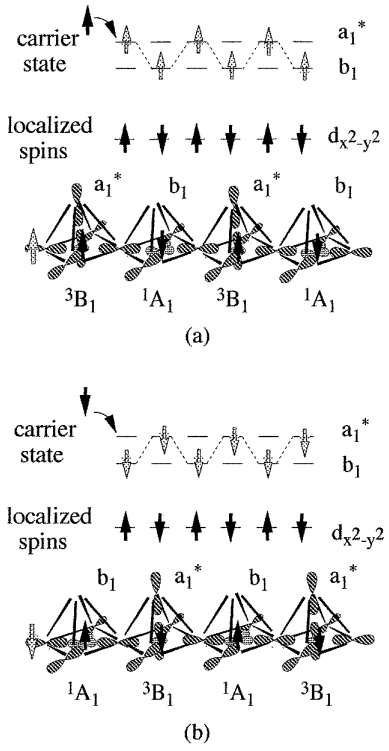

Figure 8. Schematic views of the coherent motion of a dopant hole from high-spin to low-spin states in the presence of antiferromagnetic ordering of the localized spin system in the case of superconducting $YBCO_7$. Here (a) and (b) correspond to up-spin and down-spin coherent states of dopant holes, respectively.

in a metallic state by the following forms of Bloch-type wave functions:

$$\Psi_{k\alpha}(\boldsymbol{r})\chi = \sum_{\boldsymbol{R}} \exp(\mathrm{i}\boldsymbol{k}\cdot\boldsymbol{R})[A_{\boldsymbol{k}}\phi_{\mathrm{a}^*_{1\mathrm{g}}}(\boldsymbol{r}-\boldsymbol{R}) + B_{\boldsymbol{k}}\phi_{\mathrm{b}_{1\mathrm{g}}}(\boldsymbol{r}-\boldsymbol{R}-\boldsymbol{d})]\alpha\chi \tag{4a}$$

and

$$\Psi_{-k\beta}(\boldsymbol{r})\chi = \sum_{\boldsymbol{R}} \exp(\mathrm{i}\boldsymbol{k}\cdot\boldsymbol{R})[A_{-\boldsymbol{k}}\phi_{\mathrm{a}^*_{1\mathrm{g}}}(\boldsymbol{r}-\boldsymbol{R}-\boldsymbol{d}) + B_{-\boldsymbol{k}}\phi_{\mathrm{b}_{1\mathrm{g}}}(\boldsymbol{r}-\boldsymbol{R})]\beta\chi \tag{4b}$$

where α and β represent the up- and down-spin states of a dopant hole, respectively. The spin function χ represents the antiferromagnetic ordering state of the Cu localized spins in a CuO_2 layer, where the up and down spins are assigned at $\boldsymbol{R}$ and $\boldsymbol{R}+\boldsymbol{d}$ Cu sites, respectively. Furthermore, $\boldsymbol{d}$ is a vector representing the distance between Cu sites with localized up and down spins in an antiferromagnetic unit cell. The summation over $\boldsymbol{R}$ is carried out for the antiferromagnetic unit cells. In both equations (4*a*) and (4*b*), the first and the second terms in the square brackets represent Hund's coupling and Zhang–Rice multiplets, respectively. In the case of $YBCO_7$, coherent motion of a dopant hole due to the alternate appearance of $^1A_1$ and $^3B_1$ multiplets is also possible when a CDW exists in a Cu–O chain, as shown in figure 8.

6. Experimental evidence for the increase of the spin-correlation length with the hole concentration

In the Kamimura–Suwa model, the spin-correlation length must increase in the underdoped region when the hole concentration increases, in order for every hole carrier to move over a considerable distance to form a coherent state. As to the hole concentration dependence of

the spin-correlation length, Mason *et al* [44] and Yamada *et al* [45] have recently reported independently that the spin-correlation length in the underdoped region of $La_{2-x}Sr_xCuO_4$ increases from $x = 0.05$ with increase of the hole concentration x, and reaches a value of about 50 Å for the optimum doping ($x = 0.15$). These experimental results support the Kamimura–Suwa model in which the metallic and superconducting states correspond to a coherent state characterized by the coexistence of the local spin ordering and the ordering which takes the form of the alternating appearance of $^3B_{1g}$ and $^1A_{1g}$ multiplets in the spin-correlated region.

7. The effective Hamiltonian for the Kamimura–Suwa model

The effective Hamiltonian that we use to describe the Kamimura–Suwa model consists of four parts: the effective one-electron Hamiltonian ($H_{\rm eff}$) for a^*_{1g}- and b_{1g}-orbital states, the transfer interaction between CuO_6 octahedra ($H_{\rm tr}$), the superexchange interaction between the Cu $d_{x^2-y^2}$ localized spins ($H_{\rm AF}$), and the exchange interactions between spins of dopant holes and $d_{x^2-y^2}$ holes within the same CuO_6 octahedron ($H_{\rm ex}$). Thus we have

$$\begin{aligned} H &= H_{\rm eff} + H_{\rm tr} + H_{\rm AF} + H_{\rm ex} \\ &= \sum_{i,m,\sigma} \varepsilon_m C^\dagger_{im\sigma} C_{im\sigma} + \sum_{\langle i,j\rangle,m,n,\sigma} t_{mn}(C^\dagger_{im\sigma} C_{jn\sigma} + {\rm HC}) + J \sum_{\langle i,j\rangle} \boldsymbol{S}_i \cdot \boldsymbol{S}_j \\ &\quad + \sum_{i,m} K_m \boldsymbol{s}_{i,m} \cdot \boldsymbol{S}_i \end{aligned} \tag{5}$$

where ε_m ($m = a^*_{1g}$ or b_{1g}) represents the effective one-electron energy of the a^*_{1g}- and b_{1g}-orbital states, $C^\dagger_{im\sigma}$ ($C_{im\sigma}$) the creation (annihilation) operator of a dopant hole in the ith CuO_6 octahedron, t_{mn} the effective transfer of a dopant hole between m-type and n-type orbitals of neighbouring CuO_6 octahedra, J the superexchange coupling between the spins $\boldsymbol{S}_i$ and $\boldsymbol{S}_j$ of $d_{x^2-y^2}$ localized holes in the antibonding b_{1g} orbital (b^*_{1g}) at the nearest-neighbour Cu sites i and j ($J > 0$, antiferromagnetic), and K_m the exchange integral for the exchange between the spin of a dopant hole $\boldsymbol{s}_{im}$ and the $d_{x^2-y^2}$ localized spin $\boldsymbol{S}_i$ in the ith CuO_6 octahedron ($K_{a_{1g}} < 0$ for the Hund's coupling triplet and $K_{b_{1g}} > 0$ for the Zhang–Rice singlet).

We call this model Hamiltonian of the coupled spin-fermion type the 'extended two-storey-house model', where it should be noticed that the upper-storey carrier state consists of two kinds of state, a^*_{1g} and b_{1g}, while the lower storey consists of localized spins. In this sense, the present model corresponds to a three-band system if we include the localized spin state in the lower storey, so we have used the word 'extended' in view of a previous 'two-storey-house model' proposed by Kamimura [6]. In fact, the term 'two-storey-house model' was acknowledged by Cohen [46]. In the extended two-storey-house model, each band accommodates only one kind of spin, i.e. up spin or down spin. For the energy bands of up and down spins which have exactly the same energy dispersion, the spatial distributions of the wave functions in real space are different. Thus this unusual electronic state is basically a non-Fermi liquid.

8. Energy bands, the Fermi surface, and the density of states in the superconducting state of LaSCO

Kamimura and Ushio [13, 19] have calculated an effective one-electron-type energy band structure for the upper-storey carriers from the Hamiltonian (5) by separating off the

localized spin system in the lower storey by applying the molecular-field approximation to the fourth term in equation (5). Since the spins of localized holes in b_{1g}^* orbitals form an antiferromagnetic ordering, Kamimura and Ushio have selected the unit cell in such a way that it contains two neighbouring CuO_6 octahedra, called A and B sites, and have considered the 34×34-dimensional matrix ($\widetilde{H}$) of the Hamiltonian (5), where the $2p_x$, $2p_y$, and $2p_z$ atomic orbitals for each of eight oxygen atoms and $3d_{yz}$, $3d_{xz}$, $3d_{xy}$, $3d_{x^2-y^2}$, and $3d_{z^2}$ atomic orbitals for each of two Cu atoms in the unit cell are taken as the basis functions. We have called this unit cell the 'antiferromagnetic unit cell'. The Hamiltonian matrix $\widetilde{H}$ consists of two parts, the one-electron part $\widetilde{H}_0$ and the effective-interaction part $\widetilde{H}_{\rm int}$, the latter of which includes the exchange interactions between the carrier spins in the upper storey and the localized spins in the lower storey. In the case of a dopant hole with up spin, the energy of a b_{1g}^* state in a CuO_6 octahedron with localized up spin (an A site) is taken to be lower than that in a CuO_6 cluster with localized down spin (a B site) by the Hubbard U-interaction, which is taken as 10 eV in the present case. Furthermore, the energy of an a_{1g}^* state at an A site is taken to be lower than that at a B site by Hund's coupling energy, which is 2 eV, while the energy of a b_{1g} state at a B site is taken to be lower than that at an A site by the antiferromagnetic exchange energy in the $^1A_{1g}$ state, which is 4 eV. Thus we may take $K_{a_{1g}} = -2$ eV and $K_{b_{1g}} = 4$ eV in equation (5).

In this way the essential part of the many-body interaction terms in Hamiltonian (5) is taken into account in the effective one-electron terms in the 34×34-dimensional effective-interaction part $\widetilde{H}_{\rm int}$. This kind of theoretical treatment is similar in concept to the 'LDA + U' method developed by Anisimov *et al* [47] for copper oxides, but an essential point in the present treatment developed by Kamimura and Ushio [19] is the separation of the localized spin system in the lower storey from the carrier system in the upper storey, by expressing $H_{\rm ex}$ in equation (5) as

$$\sum_{i,m} K_m \, \boldsymbol{s}_{i,m} \cdot \langle \boldsymbol{S}_i \rangle$$

by using the molecular-field approximation, where $\langle \boldsymbol{S}_i \rangle$ is the average value of a localized spin at the ith Cu site, and the inclusion of the exchange interactions between the spins in the upper and lower storeys in the effective one-electron terms for the carriers of the upper storey. As a result, all of the matrix elements in the 34×34-dimensional Hamiltonian matrix ($\widetilde{H}$) are expressed in the form of one-electron-type ones, and thus one-electron-type energy bands of carriers in the upper storey can be obtained by diagonalizing $\widetilde{H}$.

Once this has been done, all of the matrix elements related to the transfer interactions which appear in the 34×34-dimensional Hamiltonian matrix ($\widetilde{H}_0$) can be estimated from the Slater–Koster parameters determined by DeWeert *et al* [48] for La_2CuO_4. Furthermore, the value for the difference between $\varepsilon_{a_{1g}}$ and $\varepsilon_{b_{1g}}$ has been taken in such a way as to reproduce the energy difference between the multiplet states $^3B_{1g}$ and $^1A_{1g}$ calculated by Kamimura and Eto [12]. In this way, Kamimura and Ushio were able to separate the localized spin part in the lower storey from that of the upper storey, and they obtained a band structure including the many-body effects in a mean-field sense for the itinerant carriers in LaSCO. The band structure for up-spin dopant holes thus obtained is shown in figure 9, where the ordinary Brillouin zone corresponding to an ordinary unit cell which includes only one CuO_6 octahedron is also shown in the upper part of the figure. The same shape of band structure is also obtained for down-spin dopant holes. In undoped La_2CuO_4, all of the bands are occupied by electrons, so La_2CuO_4 is an insulator, which is consistent with the experimental result [22]. In figure 9 the highest occupied band is indicated by a solid line denoted as No 1. The top of the highest band is located at the Δ point in the ordinary

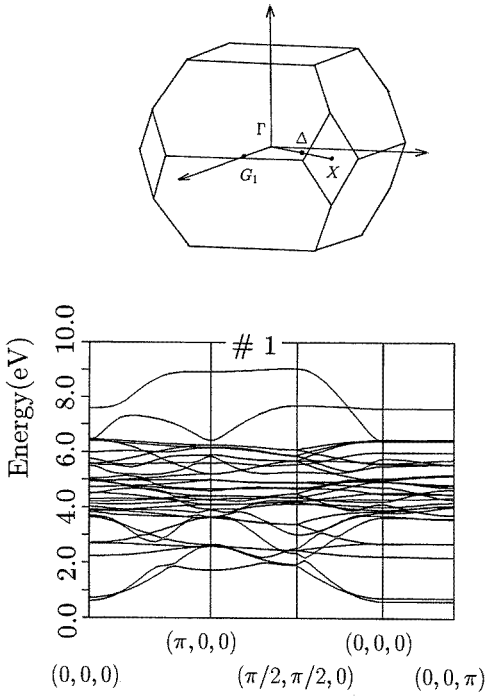

Figure 9. The band structure with the many-body effect included for up-spin dopant holes, obtained by solving the effective one-electron-type 34×34-dimensional Hamiltonian matrix $\tilde{H}$ for an antiferromagnetic unit cell; the ordinary Brillouin zone corresponding to an ordinary unit cell consisting of a single CuO_6 octahedron is shown in the upper part of the figure. The highest occupied band is marked as the No 1 band. The Δ point corresponds to $(\pi/2a, \pi/2a, 0)$, while the G_1 point corresponds to $(\pi/a, 0, 0)$. In the figure, the Cu–O–Cu distance, a, is taken to be unity.

Brillouin zone, where Δ corresponds to the edge of the antiferromagnetic Brillouin zone, $(\pi/2a, \pi/2a, 0)$, with a being the distance between neighbouring Cu sites. In this context, the present concept of the energy bands in figure 9 is completely different from the ordinary concept of energy bands in the one-electron picture, such as those calculated using the LDA.

When Sr ions are doped, holes begin to occupy the top of the highest band (No 1) at Δ. At the critical hole concentration x_0 at which the superconductivity appears, the Fermi level in the No 1 band is located at an energy much higher than that of the G_1 state, where G_1 in the Brillouin zone corresponds to $(\pi/a, 0, 0)$ and also to a singularity of the two-dimensional density of states. In figure 10 the wave functions at the Δ and G_1 points for the No 1 band are shown, where the right-hand side of the figure corresponds to a CuO_6 octahedron with localized up spin (an A site) and the left-hand side corresponds to a CuO_6 octahedron with localized down spin (a B site). One can see from this figure that for concentrations below the onset of superconductivity the holes with up spin are accommodated in b_{1g} orbitals constructed mainly from oxygen p_σ orbitals in the CuO_2 plane for the A site, which is consistent with the result of the cluster calculation by Kamimura and Eto [12], while in the superconducting concentration regime the holes move from an a^*_{1g} orbital at the A site to a b_{1g} orbital at the B site, consistently with the prediction made by Kamimura and Suwa [18]. Here it should be remarked that the mixing ratio of the Zhang–Rice singlet is always dominant for the Hund's coupling triplet. Quantitatively, the ratio of the $^1A_{1g}$ to the

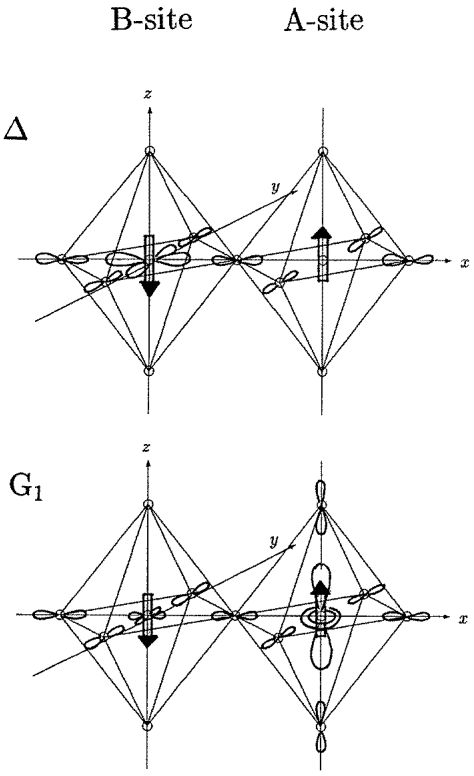

Figure 10. The wave functions at Δ and G_1 points. Here, the right-hand side of the figure corresponds to a CuO_6 cluster with localized up-spin (an A site) and the left-hand side to a CuO_6 cluster with localized down spin (a B site).

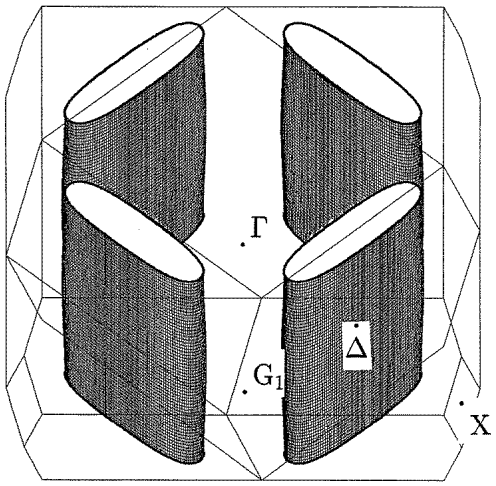

Figure 11. The Fermi surface for $x = 0.15$ calculated for the No 1 band. Here two kinds of Brillouin zone are also shown. One, the outermost part, is the ordinary Brillouin zone, and the inner part is the folded Brillouin zone for the antiferromagnetic unit cell in LaSCO. Here the k_x-axis is taken along $\overline{\Gamma G_1}$, corresponding to the x-axis (the Cu–O–Cu direction) in real space.

$^3B_{1g}$ component is at most 8:2 in the underdoped region of LaSCO, consistently with the experimental results given by Chen *et al* [14].

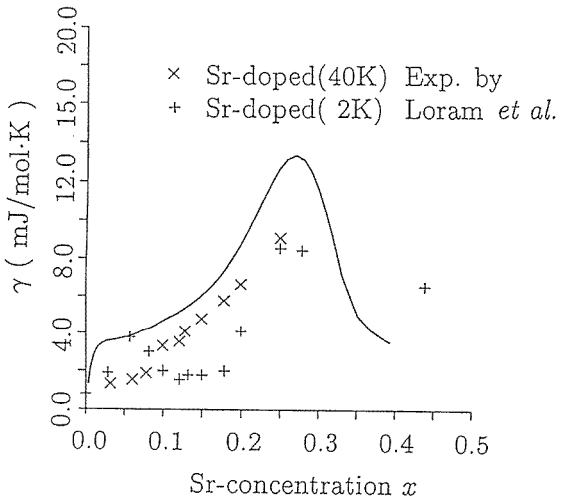

Figure 12. The electronic specific heat of LaSCO as a function of the hole concentration x. The solid lines show the results calculated for the No 1 band in the renormalized band structure [55] while the crosses show the experimental data given by Loram *et al* [56]. The energy is measured from the top of the band. Holes enter from the top.

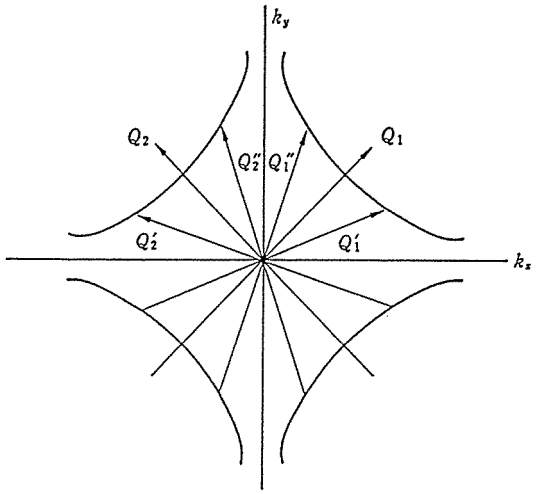

Figure 13. A way of expressing the location of the Fermi surfaces in the k_x–k_y plane in terms of the $\boldsymbol{Q}_1$- and $\boldsymbol{Q}_2$-vectors which are the bisectors of the k_x- and k_y-axes, and a schematic view of the nesting vectors $\boldsymbol{Q}_1'$, $\boldsymbol{Q}_1''$, $\boldsymbol{Q}_2'$, and $\boldsymbol{Q}_2''$ connecting the Fermi surfaces.

Kamimura and Ushio have also calculated the Fermi surfaces and the density of states of the No 1 band for LaSCO. For example, the Fermi surfaces for $x = 0.15$ calculated by them are shown in figure 11 and the density of states for the No 1 band is shown in figure 12. The Fermi surface for $x = 0.15$ consists of two pairs of extremely flat tubes, which are directed along bisectors between the k_x-axis and the k_y-axis, and are orthogonal to each other. The distance between the two Fermi surfaces facing each other and their directions are close to the $\boldsymbol{Q}_1$- and $\boldsymbol{Q}_2$-vectors shown in figure 13, where the $\boldsymbol{Q}_1$ and $\boldsymbol{Q}_2$-vectors are equivalent to the vectors $(\pi/a, \pi/a, 0)$ and $(-\pi/a, \pi/a, 0)$, respectively. The cross section of each Fermi surface facing towards the Γ point, the centre of the Brillouin zone, is very wide, and the dispersion of the highest band is relatively flat. These unique features of

the energy dispersion of the No 1 band and Fermi surfaces have been checked by angle-resolved UPS experiments for $Bi_2Sr_2CuO_6$ (Bi2201), $Bi_2Sr_2CaCu_2O_{8+\lambda}$ (Bi2212) [49–51], and $Bi_2Sr_2Ca_{1-x^2}Dy_xCu_2O_{8+\delta}$. In particular, Aebi *et al* [49, 50] have observed a $\sqrt{2} \times \sqrt{2}$ superstructure, supporting the prediction of the existence of short-range antiferromagnetic correlations made by Kamimura and Suwa. The features of the calculated Fermi surface change drastically in the overdoped region at around $x \sim 0.2$. In this overdoped region, four flat sections of the Fermi surface merge into one 'large Fermi surface.' This may explain the anomalous phenomena observed in various normal-state properties such as the pseudogap.

In connection with the features of the Fermi surfaces shown in figure 11, we would like to point out the possibility of nesting of Fermi surfaces with different spins and of nesting of those with the same spin for the nesting vectors $\boldsymbol{Q}_1'$, $\boldsymbol{Q}_1''$, $\boldsymbol{Q}_2'$, and $\boldsymbol{Q}_2''$, which deviate slightly from the commensurate $\boldsymbol{Q}_1$- and $\boldsymbol{Q}_2$-vectors, as seen in figure 13. The former type of nesting may cause anomalies in spin excitation spectra while the latter is related to anomalies in phonon spectra for the above nesting vectors. The appearance of incommensurate peaks in the spin excitation spectra of LaSCO observed in neutron diffraction experiments [52] might be related to the above anomalies.

The density of states for the No 1 band shown in figure 12 has a sharp peak at E_F corresponding to $x \sim 0.3$ in $La_{2-x}Sr_xCuO_4$. The appearance of this sharp peak is due to a two-dimensional singularity at the G_1 point, suppressed by the transfer interaction between adjacent CuO_2 layers. A similar calculation is now being made for $YBCO_7$ [53].

9. Summary, and remarks on the origin of the pseudogap

By reviewing the first-principles studies of the many-electron electronic structures of underdoped $La_{2-x}Sr_xCuO_4$ and $YBa_2Cu_3O_7$ performed by Kamimura and co-workers, unusual electronic states have been clarified. That is, the dopant holes move coherently by taking the Zhang–Rice spin singlet and Hund's coupling spin triplet alternately in the spin-correlated region of antiferromagnetic ordering due to the Cu localized spins. We have shown that this creates a metallic state which leads to superconductivity. The coexistence of (i) the antiferromagnetic spin ordering and (ii) the ordering in the appearance of the Zhang–Rice singlet and the Hund's coupling triplet is essentially important, and results in the small Fermi surface for a carrier system and the decrease in the electronic entropy below a certain temperature at which the Fermi surface changes from a larger one to smaller ones. Recently, Loram *et al* [54] concluded, from experimental results on the electronic specific heat, the electronic entropy, and the spin susceptibility, that a states-non-conserving pseudogap exists in the quasiparticle spectrum in underdoped cuprates and that the pseudogap energy reflects the energy scale of the correlated holes and spins, and is not due to superconducting fluctuations or additional competing interactions. We discuss the microscopic origin of the pseudogap from the present view of non-Fermi liquid. According to the Kamimura–Suwa model, the localized holes in the antibonding b_{1g} orbitals form an antiferromagnetic ordering in the spin-correlated region. The entropy loss observed above T_c in underdoped LaSCO is due to the formation of the local antiferromagnetic ordering mentioned above. The observed temperature dependence of the spin susceptibility in underdoped LaSCO can be explained by the contribution from the spin-correlated region of local antiferromagnetic ordering. Then the contribution to the electronic specific heat comes from the hole carriers in the small Fermi surfaces shown in figure 11. In fact, the density of states at the Fermi energy calculated by Ushio and Kamimura [55] for $La_{2-x}S_xCuO_4$ shown in figure 12 is in good agreement with that obtained from the observed electronic specific heat data given

by Loram *et al* [56] for $0.05 \leqslant x \leqslant 0.2$, as seen in figure 12. When the temperature increases to a value much higher than T_c, the spin-correlation length decreases, and thus the metallic state due to the alternating appearance of the $^1A_{1g}$ Zhang–Rice singlet and the $^3B_{1g}$ Hund's coupling triplet disappears. As a result, the small Fermi surfaces change to the large Fermi surface obtained from an ordinary band-structure calculation in the local density approximation. In this context, we conclude in view of the Kamimura–Suwa model that the origin of the pseudogap is ascribable to the change from the large Fermi surface to the small Fermi surfaces caused by the appearance of local antiferromagnetic ordering due to the presence of the Cu localized spins.

Acknowledgments

One of the authors (HK) would like to thank Dr John Loram and Professor Yao Liang for very valuable discussions on various topics mentioned in this article and for their hospitality when HK stayed at the Interdisciplinary Research Centre in Superconductivity, University of Cambridge, in March of 1998. HK also thanks Dr C T Chen for useful suggestions and discussions on the relation between the $^1A_{1g}$ and $^3B_{1g}$ multiplets and the polarized x-ray absorption spectra of LaSCO, and Dr Hideki Ushio for providing information on the wave functions on the Fermi surfaces for various concentrations of Sr in LaSCO.

References

[1] Bednorz J G and Müller K A 1986 *Z. Phys.* B **64** 189
[2] Anderson P W 1987 *Science* **235** 1196
[3] See, for example,
Kamimura H and Oshiyama A (ed) 1989 *Mechanisms of High Temperature Superconductivity (Springer Series in Materials Science 11)* (Heidelberg: Springer)
[4] See also,
Fukuyama H, Maekawa S and Malozemoff A P (ed) 1989 *Strong Correlation and Superconductivity (Springer Series in Solid-State Sciences 89)* (Heidelberg: Springer)
[5] Kamimura H, Matsuno S and Saito R 1989 *Mechanisms of High Temperature Superconductivity (Springer Series in Materials Science 11)* ed H Kamimura and A Oshiyama (Heidelberg: Springer) p 8
[6] Kamimura H 1988 *Int. J. Mod. Phys.* B **1** 699
[7] Shima N, Shiraishi K, Nakayama T, Oshiyama A and Kamimura H 1988 *Proc. 1st Int. Conf. on Electronic Materials* ed T Sugano, R P H Chang, H Kamimura, I Hayashi and T Kamiya (Pittsburgh, MA: MRS) p 51
[8] Egami T, Toby B H, Billinge S J L, Janot Chr, Jorgensen J D, Hinks D G, Subramanian M A, Crawford M K, Farneth W E and McCarron E M 1992 *High Temperature Superconductivity* ed J Ashkenazi and G Vezzoli (New York: Plenum) p 389
and related references therein
[9] Cava R J *et al* 1988 *Physica* C **153–155** 560
[10] Shmahl W W, Salje E and Liang W Y 1988 *Phil. Mag. Lett.* **58** 181
[11] Boyce J B, Bridges F, Claeson T, Geballe T H, Chu C W and Tarascon J M 1987 *Phys. Rev.* B **35** 7203
[12] Kamimura H and Eto M 1990 *J. Phys. Soc. Japan* **59** 3053
and also see
Eto M and Kamimura H 1991 *J. Phys. Soc. Japan* **60** 2311
[13] Kamimura H and Ushio H 1994 *Solid State Commun.* **91** 97
See also
Kamimura H, Eto M, Matsuno S and Ushio H 1992 *Comment. Condens. Matter Phys.* **15** 303
and related references therein
[14] Chen C T, Tjeng L H, Kwo J, Kao H L, Rudolf P, Sette F and Fleming R M 1992 *Phys. Rev. Lett.* **68** 2543
[15] Pellegrin E, Nücker N, Fink J *et al* 1993 *Phys. Rev.* B **47** 3354
[16] Bianconi A, Castrucci P, Fabrizi A, Pompa M, Flank A M, Lagarde P, Katayama-Yoshida H and Calestani G 1989 *Physica* C **162–164** 209

[17] Birgeneau R J, Endoh Y, Hidaka Y, Kakurai K, Kastner M A, Murakami T, Shirane G, Thurston T R and Yamada K 1989 *Mechanisms of High Temperature Superconductivity (Springer Series in Materials Science 11)* ed H Kamimura and A Oshiyama (Heidelberg: Springer) p 120
See also
Birgeneau *et al* 1988 *Phys. Rev.* B **38** 6614
[18] Kamimura H and Suwa Y 1993 *J. Phys. Soc. Japan* **62** 3368
[19] Ushio H and Kamimura H 1995 *J. Phys. Soc. Japan* **64** 2585
[20] Kamimura H, Matsuno S, Suwa Y and Ushio H 1996 *Phys. Rev. Lett.* **77** 723
[21] Matsuno S, Ushio H, Suwa Y and Kamimura H 1997 *Int. J. Mod. Phys.* B **32** 3815
[22] Takagi H, Ido T, Ishibashi S, Uota M, Uchida S and Tokura Y 1989 *Phys. Rev.* **40** 2254
[23] Cava R J, Santoro A, Johnson D W Jr and Rhodes W W 1987 *Phys. Rev.* B **35** 6716
We use the lattice constants at 10 K reported there.
[24] Roos B, Veillard A and Vinot G 1971 *Theor. Chim. Acta* **20** 1
[25] Dunning T H Jr and Hay P J 1977 *Methods of Electronic Structure Theory (Modern Theoretical Chemistry 3)* ed H F Schaefer III (New York: Plenum) p 1
[26] Gun Y, Langlois J and Goddard W A III 1988 *Science* **239** 896
[27] Asai Y 1989 *J. Phys. Soc. Japan* **58** 3264
[28] Yamamoto S, Yamaguchi K and Nasu K 1990 *Phys. Rev.* B **42** 266
[29] Zhang F C and Rice T M 1988 *Phys. Rev.* B **37** 3759
[30] Wahl A C and Das G 1977 *Methods of Electronic Structure Theory (Modern Theoretical Chemistry 3)* ed H F Schaefer III (New York: Plenum) p 51
[31] Kato S and Morokuma K 1979 *Chem. Phys. Lett.* **65** 19
[32] Eto M and Kamimura H 1988 *Phys. Rev. Lett.* **61** 2790
[33] Eto M and Kamimura H 1991 *J. Phys. Soc. Japan* **60** 2311
[34] Sano A, Eto M and Kamimura H 1997 *Int. J. Mod. Phys.* B **11** 3733
[35] Kamimura H and Sano A 1997 *J. Supercond.* **10** 279
[36] Shimizu T, Yasuoka H, Imai T, Tsuda T, Takabatake T, Nakazawa Y and Ishikawa M 1988 *J. Phys. Soc. Japan* **37** 2494
[37] Sano A, Eto M and Kamimura H 1997 *Int. J. Mod. Phys.* B **11** 3733
[38] Sano A 1998 *PhD Thesis* Science University of Tokyo
[39] Edward H L, Barr A L, Markert J T and de Lozanne A L 1994 *Phys. Rev. Lett.* **73** 1154
[40] Mook M A, Dai P, Salama K, Lee D, Dŏgan F, Aeppli G, Boothroyd A T and Mostoller M E 1996 *Phys. Rev. Lett.* **77** 370
[41] Grévin B, Berthier Y, Collin G and Mendels P 1998 *Phys. Rev. Lett.* **80** 2405
[42] Gagnon R, Pu S, Ellman B and Taillefer L 1997 *Phys. Rev. Lett.* **78** 1976
[43] See also
Bianconi A B and Saini N L (ed) 1997 *Proc. Int. Conf. on Stripes, Lattice Instabilities and High T_c Superconductivity; J. Supercond.* **10** (special issue)
[44] Mason T E, Schröder A, Aeppli G, Mook H A and Hayden S M 1996 *Phys. Rev. Lett.* **77** 1604
[45] Yamada K *et al* 1997 *J. Supercond.* **10** 343
[46] Cohen M L 1991 *New Horizons in Low-Dimensional Electron Systems, A Festschrift in Honour of Professor H Kamimura* ed H Aoki, M Tsukada, M Schlüter and F Levy (Dordrecht: Kluwer) p 191
[47] Anisimov V I, Korotin M A, Zaanen J and Andersen O K 1992 *Phys. Rev. Lett.* **68** 345
[48] DeWeert M J, Papaconstantopoulos D A and Pickett W E 1989 *Phys. Rev.* B **39** 4235
[49] Aebi P, Osterwalder J, Schwaller P, Schlapbach L, Shimoda M, Mochiku T and Kadowaki K 1994 *Phys. Rev. Lett.* **72** 2757
[50] Aebi P, Osterwalder J, Schwaller P, Schlapbach L, Shimoda M, Mochiku T, Kadowaki K, Berger H and Lévy F 1994 *Physica* C **235–240** 949
[51] Marshall D S *et al* 1996 *Phys. Rev. Lett.* **76** 4841
[52] Shirane G *et al* 1989 *Phys. Rev. Lett.* **63** 330
[53] Nomura K and Kamimura H 1998 in preparation
[54] Loram J W, Mirza K A, Cooper J R and Tallon J L 1998 *J. Phys. Chem. Solids* at press
and related references therein
[55] Ushio H and Kamimura H 1997 *Int. J. Mod. Phys.* B **11** 3759
[56] Loram J W, Mirza K A, Liang W Y and Osborne J 1989 *Physica* C **162–164** 498